INTRODUCTION TO BEAM-BEAM EFFECTS

H. Mais,
DESY, Hamburg, FRG

C. Mari,
ENEA, Frascati, Italy

ABSTRACT

An introduction is given to beam-beam effects in lepton and hadron colliders. The experimental results and facts are summarized and some theoretical tools and methods are explained.

1. INTRODUCTION

Lepton and hadron storage rings have become one of the most important tools in high energy physics. These storage rings are devices which allow two beams of ultrarelativistic charged particles, rotating in opposite directions to be accumulated, maintained and collided (see Fig. 1).

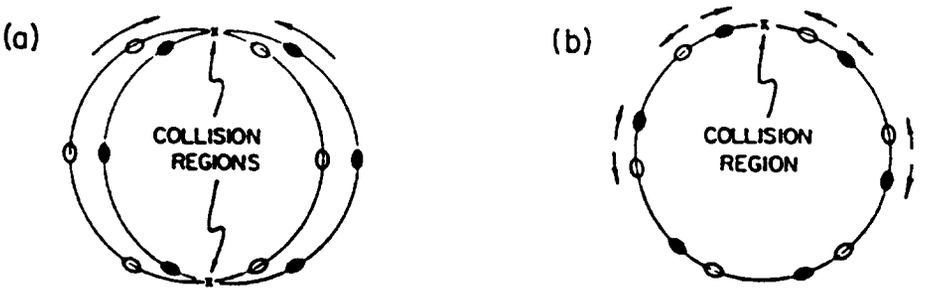

Fig. 1 Storage rings

One important difference between a collider and a conventional accelerator is that during the repeated crossing of the ultrarelativistic beams the particle motion is violently disturbed. This perturbation results in certain – mainly unwanted – effects. These so-called beam-beam effects have been the topic of special workshops and conferences [1 – 3] and are still being investigated intensively. Some review articles are [4 – 16].

This introductory lecture cannot cover the whole subject exhaustively, so we shall try to illustrate the problem, to introduce the reader to some basic facts and concepts and to explain some of the theoretical tools and methods which can be used for a quantitative formulation of the problem.

The paper is organized as follows: After a short recapitulation of the concept of luminosity and the various interaction geometries and operational modes of a storage ring, we calculate the deflection of a single particle traversing a strong beam with Gaussian charge distribution. The next section treats simple linear beam-beam models – at first we consider the perturbed linear dynamics of a single particle due to the electromagnetic fields of the counter rotating beam. The beam-beam strength parameter ξ is defined; this is used extensively in all studies of the beam-beam effect. As a second model we investigate the motion of two rigid bunches under the influence of the beam-beam interaction. In both cases a stability criterion is derived for the motion of the system. The next part summarizes the experimental facts and results for lepton and hadron colliders obtained in the past which show that the nonlinear character of the beam-beam interaction plays a very important role. The implications due to these nonlinearities are discussed next and some of the theoretical tools such as numerical simulations and analytical methods are explained. A list of unsolved problems and some comments on future colliders conclude this lecture.

2. BASIC FACTS

The reaction rate for a process of cross section σ obtained in a collider can be written as

$$R = \mathcal{L} \cdot \sigma \tag{1}$$

where $\mathcal{L}$ is the luminosity, a parameter characterizing the colliding beam system. Generally, the luminosity is calculated by integrating over all possible collisions between the particles in both beams [14,17]

$$\mathcal{L} = f_c \cdot 2c \int n_1 n_2 \, dx \, dz \, ds \, dt \tag{2}$$

where f_c is the collision frequency, c velocity of light, n_1 and n_2 are the particle densities in the two beams and the integration is over the collision region and over the time of collision, x,z designate the transverse directions and s the longitudinal direction.

The interaction geometry can be different for various storage rings. Head-on collisions are natural for particle-antiparticle single-ring colliders. Two-ring colliders generally require special design work for head-on collisions as for example HERA. Collisions with crossing angle as in DORIS I [18]or as foreseen for the SSC [19]need special care as we will point out later in this lecture.

Besides these different interaction geometries, storage rings can operate in various modes: interactions between bunched beams or interactions between continuous (coasting) beams. Furthermore strong beams can collide with strong beams or with weak beams. The latter case is approximately valid for proton-antiproton (p, $\bar{\text{p}}$) colliders.

In this lecture we will concentrate on head-on collisions of bunched beams of opposite charge. In this case the luminosity for equal beams with Gaussian charge distribution is given by

$$\mathcal{L} = \frac{N^2 \cdot f}{4\pi\sigma_x\sigma_z B} \tag{3}$$

where N is the total number of particles per beam, f the revolution frequency, B the number of bunches per beam, and σ_x, σ_z the standard deviations in x and z direction respectively.

As mentioned already, the presence of two beams which repeatedly cross each other, leads to a variety of effects in lepton and hadron colliders e.g. the blow-up of the transverse beam size which causes a loss of luminosity and a reduced beam lifetime. Figure 2 shows examples for the blow-up of the beam size of colliding electron-positron bunches in PETRA [20].

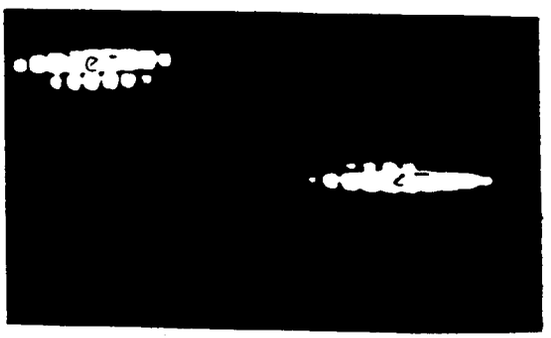

Beam dimensions at $I_{e+} = I_{e-} = 0.15mA$

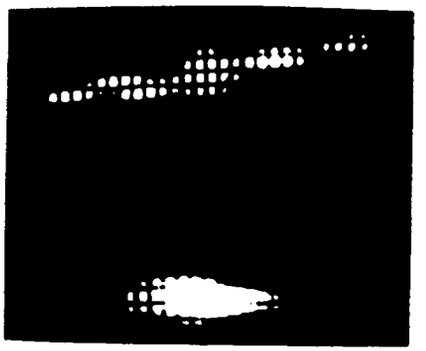

$I_{e+} = 0.52mA \quad I_{e-} = 0.74mA$

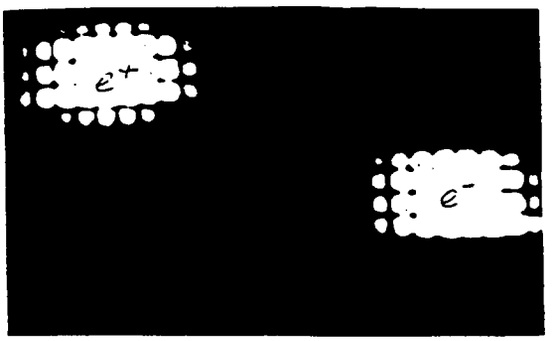

Beam dimensions at $I_{e+} = I_{e-} = 0.3mA$

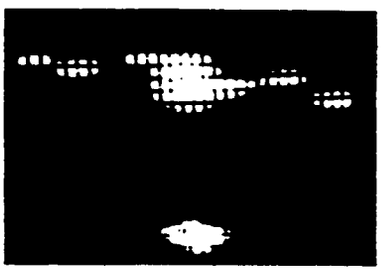

$I_{e+} = 0.6mA \quad I_{e-} = 0.6mA$

Fig. 2 Examples of beam blow-up at PETRA

Furthermore, as the beam intensity increases beyond a more or less distinct threshold one can have rapid beam loss. In hadron colliders beam-beam effects lead to emittance dilation and various diffusion effects.

So the problem one is facing in storage rings is very complicated and requires the self-consistent treatment of ultrarelativistic counter-rotating and repeatedly crossing bunches of charged particles in external electromagnetic fields in finite metallic vacuum chambers. In addition, one has to include rest-gas scattering and – at least in the lepton (e^+e^-) case – radiation effects have to be taken into account.

A general theory considering all these facts does not exist, so one usually investigates simplified models treating various aspects of the whole system. The described beam-beam effects are then related to instability mechanisms in the model under consideration.

When crossing the electromagnetic fields of the opposing beam, a particle will be deflected as illustrated in Fig. 3.

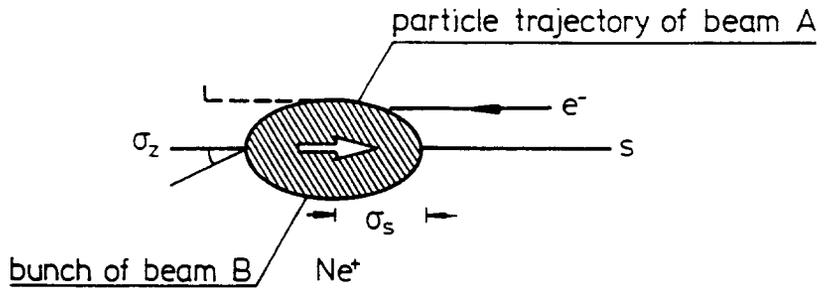

Fig. 3 Deflection of a particle because of beam-beam interaction

Once we know these fields, the deflection can be calculated by using the Lorentz equation, namely:

$$\Delta z' = \frac{\Delta p_z}{p} = -e\int_{-\infty}^{+\infty}\left(E_z + \frac{v_s}{c}B_x - \frac{v_x}{c}B_s\right)\frac{1}{p}dt \tag{4}$$

$$\Delta x' = \frac{\Delta p_x}{p} = -e\int_{-\infty}^{+\infty}\left(E_x + \frac{v_z}{c}B_s - \frac{v_s}{c}B_z\right)\frac{1}{p}dt \tag{5}$$

where $\underline{E} = (E_s, E_x, E_z)$ and $\underline{B} = (B_s, B_x, B_z)$ are the electric and magnetic fields with longitudinal and transverse components designated by s and x, z, respectively. $\underline{v} = (v_s, v_x, v_z)$ is the particle velocity and p the momentum.

In order to calculate $\underline{E}$ and $\underline{B}$ one proceeds in several steps which we shall shortly sketch. For details of the calculation the reader is referred to Refs. [21,22].

We assume a Gaussian charge distribution of the strong counter-rotating bunch with standard deviations σ_x, σ_z, σ_s in the laboratory system:

$$\varrho(x,z,s) = \frac{N_b \cdot e}{(2\pi)^{3/2}\sigma_x\sigma_z\sigma_s}\ \exp\left\{-\frac{x^2}{2\sigma_x^2} - \frac{z^2}{2\sigma_z^2} - \frac{s^2}{2\sigma_s^2}\right\} \tag{6}$$

where N_b is the number of particles per bunch.

In addition to this Gaussian charge distribution we require that the beta-function of the storage ring does not change appreciably along the bunch length, i.e.

$$\beta_0(s) = \beta_0^* + \frac{s^2}{\beta_0^*} \tag{7}$$

implies that

$$\sigma_s << \beta_0^* \tag{8}$$

where β_0^* is the value of the beta function at the interaction point.

In the center-of-mass system (u, v, w) the charge density is given by

$$\varrho(u,v,w) = \frac{N_b \cdot e}{(2\pi)^{3/2}\sigma_x\sigma_z(\gamma\sigma_s)}\ \exp\left\{-\frac{u^2}{2\sigma_x^2} - \frac{v^2}{2\sigma_z^2} - \frac{w^2}{2\gamma^2\sigma_s^2}\right\} \tag{9}$$

where γ Lorentz factor $= (1 - \frac{v^2}{c^2})^{-1/2}$.

The potential corresponding to this charge distribution can be calculated and the electric field of the Gaussian bunch is obtained in the center-of-mass system. Transforming the field back to the laboratory system using the well-known transformation rules

$$\begin{cases} E_x = \gamma E_u & E_z = \gamma E_v \qquad E_s = E_w \\ \\ B_x = \frac{v}{c}\gamma E_v & B_z = -\frac{v}{c}\gamma E_u \quad B_s = 0 \end{cases} \tag{10}$$

and taking into account (4) and (5) one finally gets for short bunches

$$\Delta z' = -\frac{2N_b r_e z}{\gamma}\int_0^\infty \frac{\exp\left\{-\frac{x^2}{2\sigma_x^2+q}-\frac{z^2}{2\sigma_z^2+q}\right\}}{(2\sigma_z^2+q)^{3/2}(2\sigma_x^2+q)^{1/2}}\,dq \tag{11}$$

$$\Delta x' = -\frac{2N_b r_e x}{\gamma}\int_0^\infty \frac{\exp\left\{-\frac{x^2}{2\sigma_x^2+q}-\frac{z^2}{2\sigma_z^2+q}\right\}}{(2\sigma_z^2+q)^{1/2}(2\sigma_x^2+q)^{3/2}}\,dq \tag{12}$$

with $r_e = \frac{e^2}{m_0 c^2}$ classical particle radius.

Remark i: The kicks experienced by the test particle can be derived from a potential $U(x,z)$

$$\begin{cases} \Delta z' = -\frac{\partial U(x,z)}{\partial z} \\ \\ \Delta x' = -\frac{\partial U(x,z)}{\partial x} \end{cases} \tag{13}$$

$$U(x,z) = \frac{N_b r_e}{\gamma}\int_0^\infty \frac{1-\exp\left\{-\frac{x^2}{2\sigma_x^2+q}-\frac{z^2}{2\sigma_z^2+q}\right\}}{(2\sigma_z^2+q)^{1/2}(2\sigma_x^2+q)^{1/2}}\,dq. \tag{14}$$

Remark ii: In the limiting case of round beams with $\sigma_x = \sigma_z = \sigma$ Eqs. (11) and (12) can be evaluated easily giving

$$\begin{cases} \Delta z' = -\frac{2N_b r_e z}{\gamma r^2}(1 - \exp\,(-r^2/2\sigma^2)) \\ \Delta x' = -\frac{2N_b r_e x}{\gamma r^2}(1 - \exp\,(-r^2/2\sigma^2)) \end{cases} \tag{15}$$

$$(r^2 = x^2 + z^2).$$

Fig. 4 shows schematically the beam-beam kick as a function of displacement

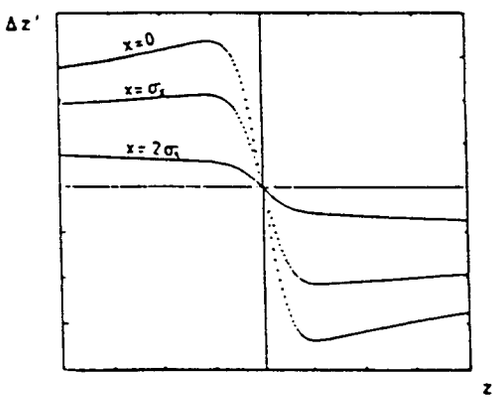

Fig. 4 Beam-beam kick as a function of displacement

For small values $x << \sigma_x, z << \sigma_z$ the behaviour is linear. Using (11) and (12) one obtains

$$\Delta z' = -\frac{2N_b r_e z}{\gamma(\sigma_x + \sigma_z)\sigma_z} = -\frac{1}{f_z} \cdot z \tag{16}$$

$$\Delta x' = -\frac{2N_b r_e x}{\gamma(\sigma_x + \sigma_z)\sigma_x} = -\frac{1}{f_x} \cdot x \tag{17}$$

with

$$\frac{1}{f_z} = \frac{2N_b r_e}{\gamma(\sigma_x + \sigma_z)\sigma_z} \tag{18}$$

$$\frac{1}{f_x} = \frac{2N_b r_e}{\gamma(\sigma_x + \sigma_z)\sigma_x}. \tag{19}$$

3. LINEAR BEAM-BEAM MODELS

As a simple model we now study the dynamics of a test particle which is perturbed by the linear beam-beam kicks. The interaction point s_{ip} is specified by ($y = x$ or z)

$$y(s_{ip} + \varepsilon) = y(s_{ip} - \varepsilon) \tag{20}$$

$$y'(s_{ip} + \varepsilon) = y'(s_{ip} - \varepsilon) - \frac{1}{f_y} y(s_{ip} - \varepsilon) \tag{21}$$

or in matrix notation:

$$\begin{pmatrix} y(s_{ip} + \varepsilon) \\ y'(s_{ip} + \varepsilon) \end{pmatrix} = \begin{pmatrix} 1 & 0 \\ -\frac{1}{f_y} & 1 \end{pmatrix} \begin{pmatrix} y(s_{ip} - \varepsilon) \\ y'(s_{ip} - \varepsilon) \end{pmatrix} \tag{22}$$

The 2×2 matrix describing the beam-beam interaction in this linear model is equivalent to the transfer matrix of a thin lens quadrupole of focal length f_y [23]. The influence of this additional perturbation on the particle motion can be calculated in the usual way [23].

For symmetry reasons we will split the beam-beam kick into two halves as sketched in Fig. 5.

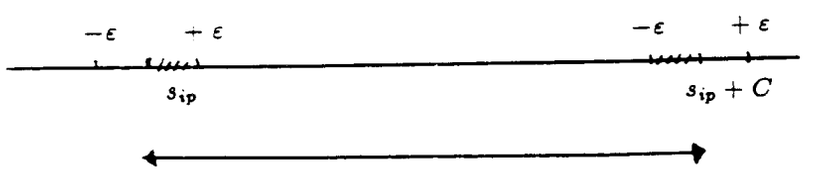

half beam-beam kick half beam-beam kick

(C distance between two adjacent interaction points)

Fig. 5

The transfer matrix from one interaction point to the next interaction point is then given by:

$$\begin{pmatrix} \cos(\mu_y + \Delta\mu_y) & \beta_y^* \sin(\mu_y + \Delta\mu_y) \\ -\frac{1}{\beta_y^*} \sin(\mu_y + \Delta\mu_y) & \cos(\mu_y + \Delta\mu_y) \end{pmatrix} = \begin{pmatrix} 1 & 0 \\ -\frac{1}{2f_y} & 1 \end{pmatrix} \begin{pmatrix} \cos\mu_y & \beta_{0y}^* \sin\mu_y \\ -\frac{1}{\beta_{0y}^*} \sin\mu_y & \cos\mu_y \end{pmatrix} \begin{pmatrix} 1 & 0 \\ -\frac{1}{2f_y} & 1 \end{pmatrix} \tag{23}$$

$(\mu_y + \Delta\mu_y)$, β_y^* are the perturbed lattice functions (phase advance between interaction points and beta function). As usual we assume that β' vanishes at the interaction point.
$\Delta\mu_y$ is calculated from

$$\begin{aligned} \cos(\mu_y + \Delta\mu_y) &= \cos\mu_y - \frac{\beta_{0y}^*}{2f_y} \sin\mu_y \\ &= \cos\mu_y - 2\pi \cdot \xi_y \sin\mu_y \end{aligned} \tag{24}$$

where we have introduced the beam-beam strength parameter

$$\xi_y = \frac{N_b r_e \beta_{0y}^*}{2\pi\,\gamma\sigma_y(\sigma_x + \sigma_z)}. \tag{25}$$

ξ_y plays a fundamental role in the investigations of the beam-beam interaction. It characterizes the strength of the interaction and for small $\Delta\mu_y$ it gives the tune shift of the system due to the perturbing beam-beam kick

$$\xi_y = \frac{\Delta\mu_y}{2\pi} = \Delta Q_y. \tag{26}$$

It is straightforward to investigate the stability of the particle motion in this case. The motion is stable if the eigenvalues of the transfer matrix (23) lie on the complex unit circle which implies that the trace of (23) is less than 2, i.e.

$$|\cos\mu_y - 2\pi\xi_y \sin\mu_y| \leq 1 \tag{27}$$

or equivalently

$$\xi_y \leq \frac{1}{2\pi}\ \mathrm{cotg}\left(\frac{\mu_y}{2}\right). \tag{28}$$

The stability condition (28) is plotted in Fig. 6

Until now we have only investigated how the dynamics of a single particle is modified by a strong counter-rotating beam (incoherent effects). As a second model we study how the bunches as a whole, and described as rigid charge distributions, are influenced by the beam-beam interaction (coherent beam-beam effects) [9,13,24,25].

In order to keep the mathematics as simple as possible we only consider a storage ring with two oppositely circulating bunches. These two bunches have small center-of-mass motion in the y-direction (y = x or z). The kicks given to the two rigid bunches are computed by averaging the kicks over the bunch distribution. For a Gaussian distribution one obtains in the linear approximation

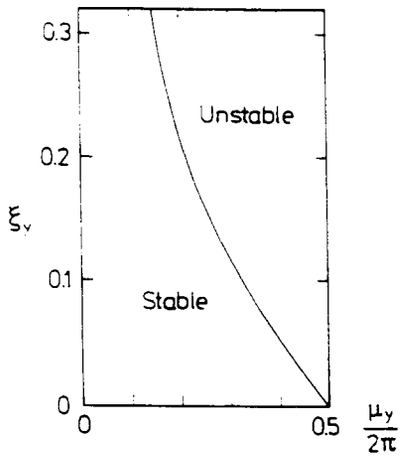

Fig. 6 Stability condition of Eq. (28)

$$\Delta y_1' = -\frac{1}{f_y}(y_1 - y_2) \cdot \frac{1}{\sqrt{2}} \tag{29a}$$

$$\Delta y_2' = -\frac{1}{f_y}(y_2 - y_1) \cdot \frac{1}{\sqrt{2}}. \tag{29b}$$

(The factor $\frac{1}{\sqrt{2}}$ is due to the averaging over a Gaussian distribution; in the case of a uniform beam $\frac{1}{\sqrt{2}}$ has to be replaced by 1 [9]). y_1 and y_2 describe the center-of-mass motion of beam 1 and 2 respectively. In matrix notation the beam-beam interaction is given by

$$\begin{pmatrix} y_1(s_{ip}+\varepsilon) \\ y_1'(s_{ip}+\varepsilon) \\ y_2(s_{ip}+\varepsilon) \\ y_2'(s_{ip}+\varepsilon) \end{pmatrix} = \begin{pmatrix} 1 & 0 & 0 & 0 \\ -\frac{1}{\sqrt{2}f_y} & 1 & \frac{1}{\sqrt{2}f_y} & 0 \\ 0 & 0 & 1 & 0 \\ \frac{1}{\sqrt{2}f_y} & 0 & -\frac{1}{\sqrt{2}f_y} & 1 \end{pmatrix} \begin{pmatrix} y_1(s_{ip}-\varepsilon) \\ y_1'(s_{ip}-\varepsilon) \\ y_2(s_{ip}-\varepsilon) \\ y_2'(s_{ip}-\varepsilon) \end{pmatrix} \tag{30}$$

After the collision the bunches execute free (linear) betatron motion for half a revolution described by

$$T_0 = \begin{pmatrix} \cos\mu_y & \beta_{0y}^* \sin\mu_y & 0 & 0 \\ -\frac{1}{\beta_{0y}^*}\sin\mu_y & \cos\mu_y & 0 & 0 \\ 0 & 0 & \cos\mu_y & \beta_{0y}^*\sin\mu_y \\ 0 & 0 & -\frac{1}{\beta_{0y}^*}\sin\mu_y & \cos\mu_y \end{pmatrix} \tag{31}$$

Combining (30) and (31) one obtains the motion for half a revolution

$$T_{t0t} = T_0 \cdot T_{BB} \tag{32}$$

with T_{BB} the 4×4 matrix from (30).

The motion of this coupled two-bunch system is stable if the eigenvalues λ of T_{t0t} lie on the complex unit circle. The eigenvalue equation for (32) can be written in the form [26]:

$$\Lambda^2 - \Lambda(4\cos\mu_y - 2\varepsilon\beta^*_{0y}\sin\mu_y) + (2\cos\mu_y - \varepsilon\beta^*_{0y}\sin\mu_y)^2 - \varepsilon^2{\beta^*_{0y}}^2\sin^2\mu_y = 0 \qquad (33)$$

where we have used the abbreviations

$$\varepsilon = \frac{1}{\sqrt{2}f_y}$$

$$\Lambda = \lambda + \frac{1}{\lambda}.$$

The solution of (33) gives four eigenvalues:

$$\lambda_{I,II} = e^{\pm i\mu_y} \qquad (34a)$$

$$\lambda_{III,IV} = e^{\pm i(\mu_y + \Delta\mu_y)} \qquad (34b)$$

where $\Delta\mu_y$ is determined by

$$\cos(\mu_y + \Delta\mu_y) = \cos\mu_y - \frac{4\pi}{\sqrt{2}}\xi_y\sin\mu_y. \qquad (35)$$

The motion belonging to (34a) is always stable and is called the σ-mode. In this mode the bunches oscillate in phase moving up and down together at the collision point. The motion corresponding to (34b) is stable if

$$|\cos\mu_y - \frac{4\pi\xi_y}{\sqrt{2}}\sin\mu_y| < 1 \qquad (36)$$

or equivalently

$$\xi_y < \frac{1}{2\sqrt{2}\pi}\ \mathrm{cotg}\ (\frac{\mu_y}{2}). \qquad (37)$$

In this case the bunches oscillate out of phase, colliding at an offset changing from collision to collision. This mode is called π-mode. This behaviour is similar to the motion of two coupled linear oscillators in classical mechanics. Figure 7 shows the stability condition (37) which is more stringent than in the incoherent case (28).

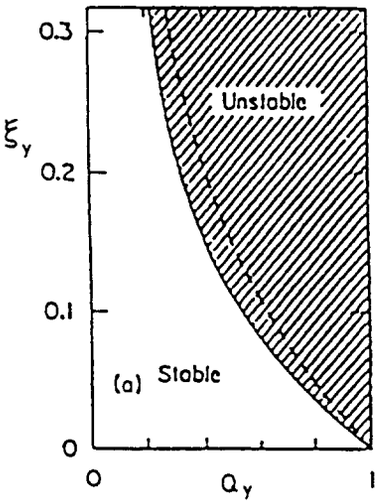

Fig. 7 Stability region for two strong rigid beams executing small center of mass oscillations as a function of the total tune Q_y of the storage ring. The dashed line shows the strong-weak stability limit of Eq. (28).

Remark i: For a uniform charge distribution the stability is given by

$$\xi_y < \frac{1}{4\pi} \ \mathrm{cotg} \ (\frac{\mu_y}{2}) \tag{38}$$

and the tune shift for small $\Delta\mu_y$ is given by

$$\Delta Q_y = \frac{\Delta\mu_y}{2\pi} = 2 \cdot \xi_y \tag{39}$$

(twice the incoherent tune shift).

Remark ii: These coherent modes have been excited and detected in various colliders. A measurement performed at PETRA is shown in Fig. 8 [20,32].

Fig. 8 Vertical eigenfrequencies of two colliding bunches

Remark iii: It is instructive to re-derive the values of the tune shifts in a different way by using perturbative methods. We will only sketch the derivation leaving the details to the reader. For a description of this perturbative approach see Ref. [27]. Using

$$\underline{z}^T = (y_1, y_1', y_2, y_2') \tag{40}$$

the equations of motion for the coupled bunch system can be written in the form

$$\frac{d}{ds}\underline{z} = (\underline{\underline{A}} + \delta\underline{\underline{A}})\underline{z} \tag{41}$$

where $\underline{\underline{A}}$ describes the unperturbed betatron motion and

$$\delta\underline{\underline{A}} = \frac{1}{\sqrt{2}} \begin{pmatrix} 0 & 0 & 0 & 0 \\ -\frac{1}{f_y} & 0 & \frac{1}{f_y} & 0 \\ 0 & 0 & 0 & 0 \\ \frac{1}{f_y} & 0 & -\frac{1}{f_y} & 0 \end{pmatrix} \cdot \delta(s - s_{ip}) \tag{42}$$

specifies the beam-beam interaction.

Equation (41) is solved by the transfer matrix (from one interaction point to the adjacent interaction point):

$$\underline{\underline{M}}(s_{ip} + C, s_{ip}) = \underline{\underline{M}}_0(s_{ip} + C, s_{ip}) + \delta\underline{\underline{M}}(s_{ip} + C, s_{ip}) \tag{43}$$

with

$$\delta \underline{\underline{M}}(s_{ip}+C, s_{ip}) = \underline{\underline{M}}_0(s_{ip}+C, s_{ip}) \times$$
$$\times \int_{s_{ip}}^{s_{ip}+C} ds' \, \underline{\underline{M}}_0^{-1}(s', s_{ip}) \delta \underline{\underline{A}}(s') \cdot \underline{\underline{M}}_0(s', s_{ip}). \tag{44}$$

In order to calculate the eigenvalues of $\underline{\underline{M}}$ we need to know the unperturbed eigenvalues of $\underline{\underline{M}}_0$ where the two bunches are uncoupled. It is easy to verify that

$$\begin{cases} \lambda_I = \lambda_{III} = e^{i\mu_y} \equiv \lambda \\ \lambda_{II} = \lambda_{IV} = \lambda^* \end{cases} \tag{45}$$

with the corresponding eigenvectors

$$\underline{v}_I = \frac{1}{\sqrt{2\beta_{0y}^*}} \begin{pmatrix} \beta_{0y}^* \\ i \\ 0 \\ 0 \end{pmatrix} \tag{46a}$$

$$\underline{v}_{III} = \frac{1}{\sqrt{2\beta_{0y}^*}} \begin{pmatrix} 0 \\ 0 \\ \beta_{0y}^* \\ i \end{pmatrix} \tag{46b}$$

and

$$\underline{v}_{II} = \underline{v}_I^*, \; \underline{v}_{IV} = \underline{v}_{III}^* \tag{47}$$

are solutions to

$$\underline{\underline{M}}_0(s_{ip}+C, s_{ip}) \underline{v}(s_{ip}) = \lambda \underline{v}(s_{ip}) \tag{48}$$

or explicitly:

$$\begin{pmatrix} \cos\mu_y & \beta_{0y}^* \sin\mu_y & 0 & 0 \\ -\frac{1}{\beta_{0y}^*}\sin\mu_y & \cos\mu_y & 0 & 0 \\ 0 & 0 & \cos\mu_y & \beta_{0y}^*\sin\mu_y \\ 0 & 0 & -\frac{1}{\beta_{0y}^*}\sin\mu_y & \cos\mu_y \end{pmatrix} \underline{v}(s_{ip}) = \lambda \underline{v}(s_{ip}).$$

The eigenvectors (46a) and (46b) satisfy the following normalisation condition [28].

$$\frac{1}{i} \underline{v}_k^+ \underline{\underline{S}} \underline{v}_\ell = \delta_{k\ell} \tag{49}$$

where $+$ means Hermitean conjugation and $\underline{\underline{S}}$ is defined by

$$\underline{\underline{S}} = \begin{pmatrix} 0 & -1 & 0 & 0 \\ 1 & 0 & 0 & 0 \\ 0 & 0 & 0 & -1 \\ 0 & 0 & 1 & 0 \end{pmatrix} \tag{50}$$

From (45) it follows that the unperturbed spectrum of $\underline{\underline{M}}_0$ is degenerate and therefore the tune shifts are calculated according to the well-known quantum mechanical expressions

$$\delta\lambda = \frac{1}{2}\left[\delta M_{11} + \delta M_{33}\right] \pm \frac{1}{2}\sqrt{(\delta M_{11} - \delta M_{33})^2 + 4\delta M_{13}^2} \tag{51}$$

where

$$\delta M_{kj} = \frac{\lambda}{i} \int_{s_{1p}}^{s_{1p}+C} ds' \underline{v}_k^+(s') \underline{\underline{S}} \delta \underline{\underline{A}}(s') \underline{v}_j(s'). \tag{52}$$

Substituting (46a), (46b), (47), (42) into (52) and solving (51) we get the results

$$\begin{cases} \delta\lambda = 0 \\ \delta\lambda = +\frac{\lambda}{i} \frac{\beta_{0y}^*}{\sqrt{2} f_y} \end{cases} \tag{53}$$

or equivalently

$$\begin{cases} \delta Q = 0 \\ \delta Q = +\frac{\beta_{0y}^*}{2\pi\sqrt{2} f_y} \end{cases} \tag{54}$$

in accordance with (36).

Remark iv: This study of rigid bunch motion under the influence of the beam-beam interaction can be extended to more bunches per beam.

A stability diagram for six colliding bunches is shown in Fig. 9.

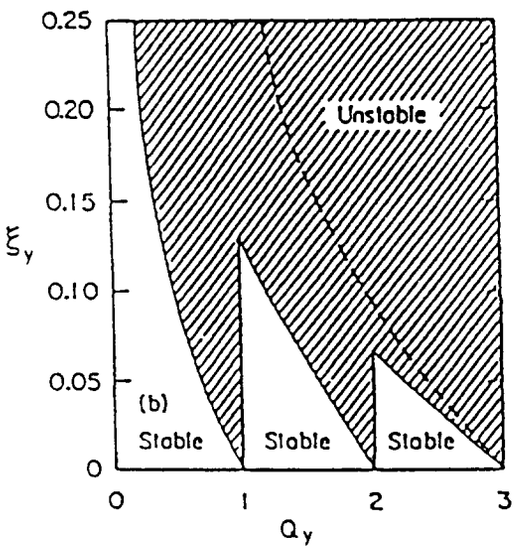

Fig. 9: Stability diagram for two strong, rigid beams executing small center-of-mass oscillations as a function of the total tune of the storage ring. Case of six colliding bunches [9,13].

Remark v: Higher order effects dealing with changes in the bunch shape have been studied in a water-bag model by Chao and Ruth [33].

4. EXPERIMENTAL FACTS AND RESULTS FOR LEPTON AND HADRON COLLIDERS

In the past 20 years the beam-beam effect has been studied intensively in many lepton storage rings. For a comprehensive review we refer the reader to Ref. [14].

In order to investigate the parameter dependence of the luminosity of a collider, we rewrite $\mathcal{L}$ as:

$$\mathcal{L} = \frac{I^2}{4\pi e^2 f B \sigma_x \sigma_z} = \frac{I\gamma\xi_z}{2er_e\beta^*_{0z}}(1+\frac{\sigma_z}{\sigma_x}) \tag{55}$$

where we have used

$$I = N \cdot ef = N_b \cdot ef \cdot B \tag{56}$$

(total current)

and

$$\xi_z = \frac{Ir_e\beta^*_{0z}}{2\pi\gamma Bef\sigma_z(\sigma_x+\sigma_z)}. \tag{25}$$

In all lepton colliders $\sigma_z << \sigma_x$ therefore one can neglect (σ_z/σ_x) in (55).

The current I of a collider depends on single-beam instabilities and coupled-bunch instabilities. Due to the chromaticity compensating sextupoles the value of β^*_{0z} is limited by aperture considerations and because of (8) by the bunch length. ξ_z depends on various operating conditions such as energy, tune of the machine, coupling, dispersion, radiation damping and all kinds of perturbations. Some important facts which have been found experimentally are listed below:

Fact i: For a beam current smaller than a characteristic threshold current I_{th}, the luminosity $\mathcal{L}$ is proportional to I^2 which implies

$$\xi_z \sim I. \tag{57}$$

For currents of the order of I_{th}, $\mathcal{L}$ varies linearly with I implying a saturation of ξ_z. This saturation is due to a linear increase of the beam size with current. For all existing lepton colliders

$$\xi_z \leq 0.07 \tag{58}$$

the so-called beam-beam limit. The dependence of $\mathcal{L}$ on I for several colliders is shown in Fig. 10 taken from Ref. [14].

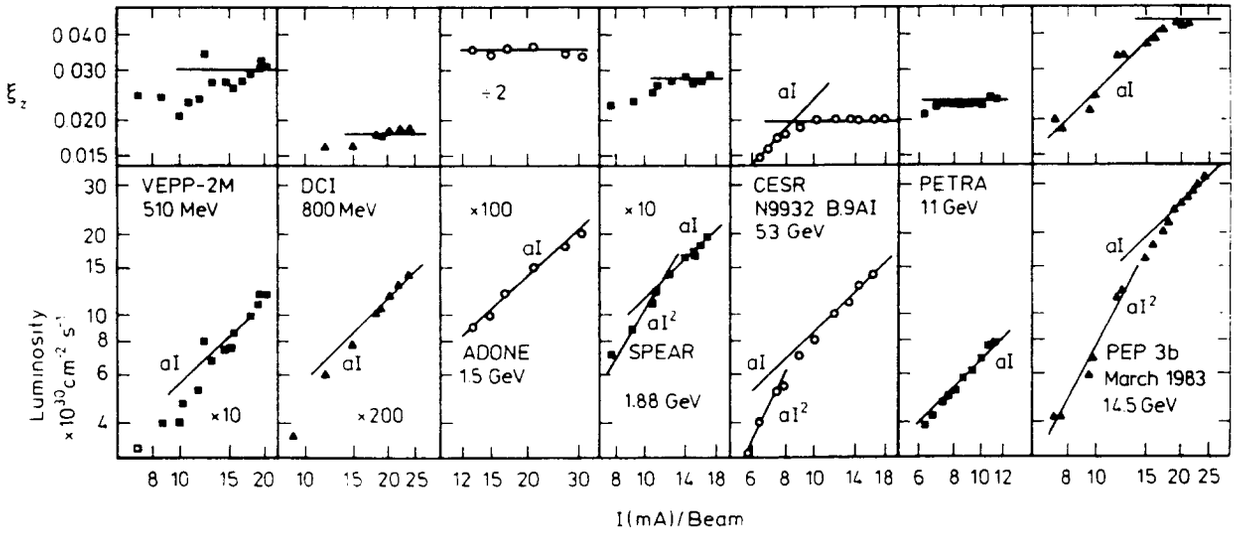

Fig. 10 Luminosity and vertical tune-shift parameter versus current for seven electron-positron colliders. Note that the tune shift saturates at some current value above which the luminosity grows linearly.

Fact ii: The performance of a collider and the luminosity depend sensitively on the working point in the tune diagram. Due to the nonlinear character of the beam-beam interaction (see Eqs. (11) and (12)) various nonlinear resonances

$$nQ_x + mQ_z = p \tag{59}$$

are present. $|n| + |m|$ characterizes the order of the resonance (n, m, p are integers). The influence of these resonances has been nicely demonstrated in an experiment performed at ACO [29]which shows the beam blow-up of a weak beam crossing a strong counter-rotating beam as one changes the tune of the machine, (see Fig. 11).

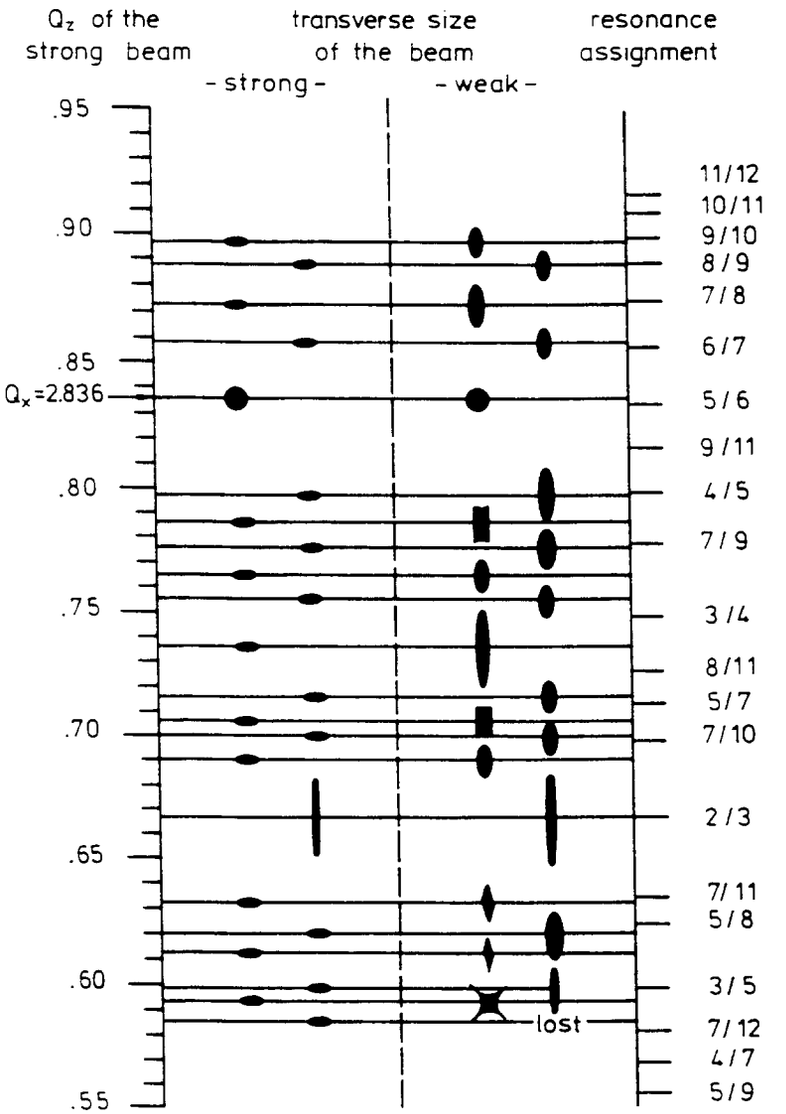

Fig. 11 Crossing of nonlinear resonances for strong-weak counter rotating beams.

Fact iii: The particle distribution in a beam is changed due to the nonlinear beam-beam interaction, (see Fig. 12 which shows scraper measurements for SPEAR [30]). A theoretical analysis and model should try to explain these results. We will come to this point later.

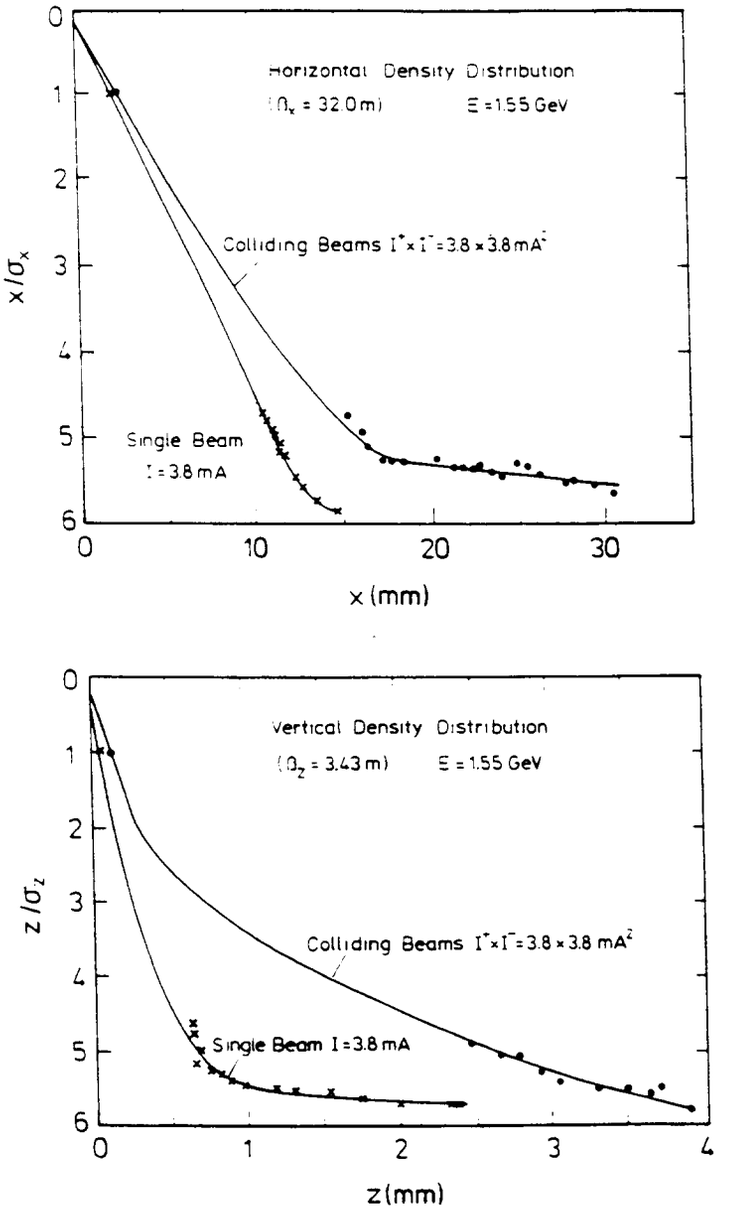

Fig. 12 Horizontal and vertical particle density distribution at SPEAR

Next let us mention the experimental situation in hadron colliders. Much less information is available in this case because there are only two $p, \bar{p}$ colliders existing at present. The main parameters and performance results are summarized in Table 1 [31]. The experience with these colliders has shown that nonlinear resonances play a dominant role and that even high-order resonances of order 10 up to 16 must be avoided. Besides the presence of these nonlinear resonances there is a further complication: In a nonlinear accelerator the tune is amplitude dependent and thus occupies a certain area in the tune diagram due to the amplitude distribution in the beam. Schematically this amplitude dependence for the beam-beam nonlinearity is depicted in Fig. 13.

	CERN S $p\bar{p}$ S	FERMILAB TEVATRON
Single beam energy (GeV)	315	900
Record peak luminosity $\times 10^{30} cm^{-2} s^{-1}$	2.49	2.06
Bunches per beam	6	6
Protons per bunch $\times 10^{10}$	11	7
Antiprotons per bunch $\times 10^{10}$	5	2.5
Crossing per circulation	3	12
Total ΔQ_z protons	0.011	0.018
Total ΔQ_z antiprotons	0.011	0.025

Table 1: Hadron colliders

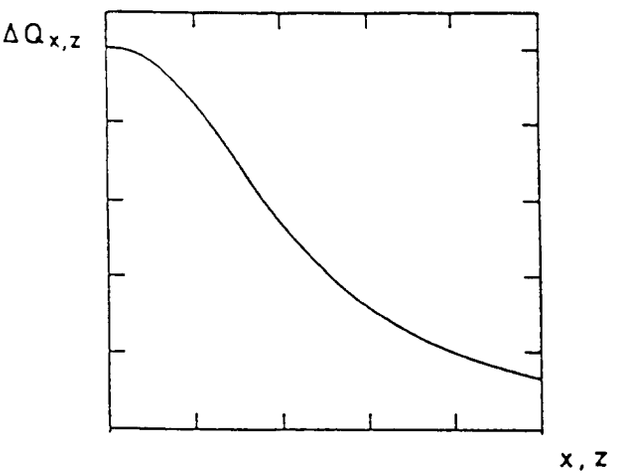

Fig. 13 Beam-beam detuning

Since the maximum ΔQ that can be accommodated in the tune diagram avoiding resonances up to order 16 is roughly 0.02 (see Fig. 14 where we show the working point for the Tevatron in the tune diagram) we obtain in this case for ξ^{Max}

$$\Delta Q \approx 0.02 \approx n \cdot \xi^{Max} \tag{60}$$

where n is the number of crossings per revolution.

This gives

$$\xi^{Max} \approx 0.002 \ldots 0.005. \tag{61}$$

These low values of ξ^{Max} (58) and (61) can not be explained with our simple linear models discussed above, thus proving that the nonlinear character of the beam-beam interaction is playing a fundamental role. In the next section we will study numerical and analytical methods to formulate the problem quantitatively.

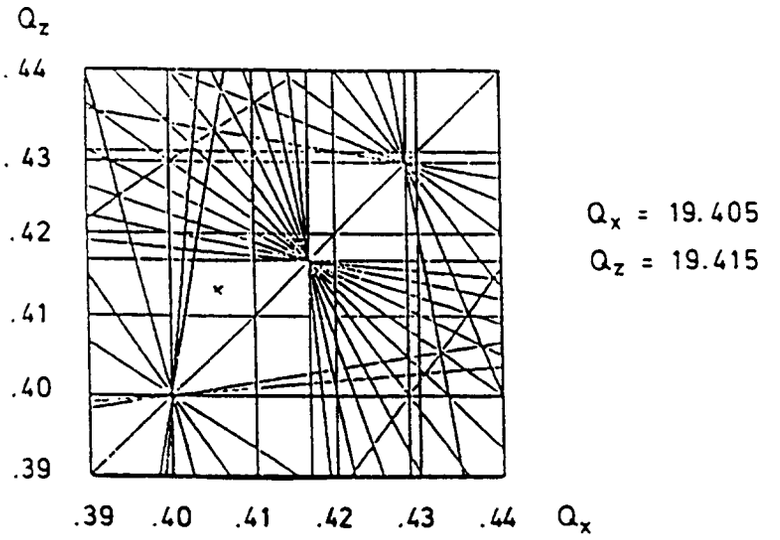

Fig. 14 Fermilab working point

5. THEORETICAL TOOLS AND METHODS

Various analytical and numerical methods have been developed to explain the experimental facts described in the last section. Numerical simulations are divided into strong-strong and weak-strong varieties. At present, simulation is the only quantitative method to study the beam-beam interaction self-consistently and to calculate the luminosity.

For lepton colliders these simulations [15,34,35,36]have to include the coupled synchro-betatron motion (six-dimensional phase space), the nonlinear beam-beam kicks, radiation damping, quantum fluctuations due to the stochastic emission of synchrotron radiation and – if necessary – other lattice or rf nonlinearities. Some results of these calculations are shown in Fig. 15 for CESR (taken from [35]) and in Fig. 16 for PETRA (taken from [34]).

The latter case shows the sensitive dependence of the beam size on perturbations of the machine. Perturbations can be small differences in betatron phase advance between the interaction points and spurious dispersion at the interaction points. Because of these numerical results a different working point was chosen for PETRA. Furthermore these simulations are very helpful for understanding the complicated interplay of nonlinearity, damping and stochastic excitation in lepton colliders. Fig. 17 taken from [37]shows such a calculation (weak-strong simulation). The combined effect of quantum fluctuations and nonlinearity can move a particle starting near the origin in phase space to a (nonlinear) resonance island before it is damped again and eventually pushed to another resonance nearby.

Analytical methods for (e^+, e^-) machines have to include the radiation effects. In this case the equations of motion are given by a system of stochastic differential equations of the form [28]:

$$\underline{x}' = \underline{A}(\underline{x}, s) + \underline{\underline{B}}(\underline{x}, s)\underline{\eta}(s) \qquad (62)$$

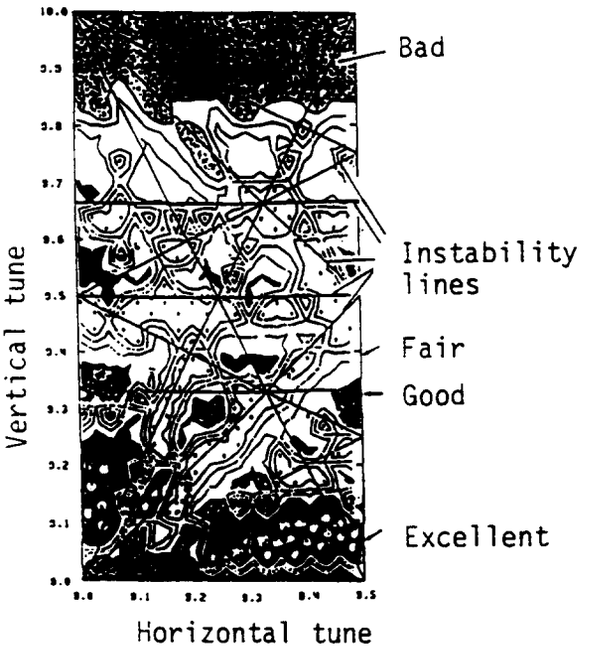

Fig. 15 Beam-beam simulation results for CESR. The contours are at equally spaced relative levels of luminosity. Crosses indicate bad lifetime. The straight lines define the positions of strong nonlinear resonances.

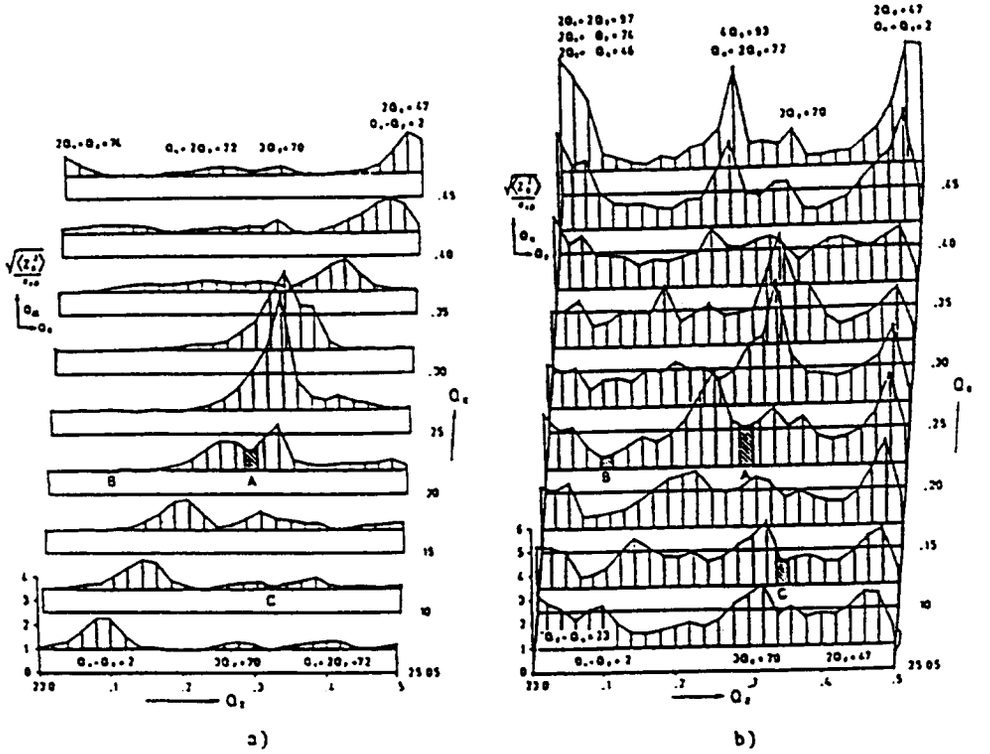

Fig 16 Simulated vertical beam height in PETRA as a function of vertical and horizontal tunes a) without machine imperfections and b) with small imperfections.

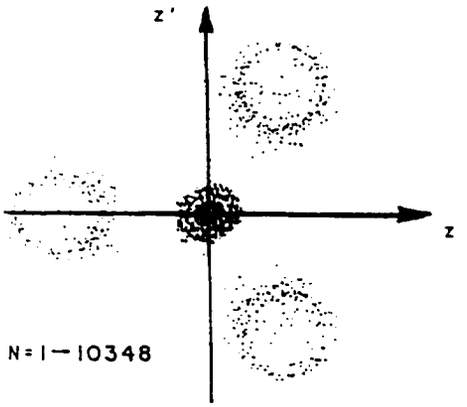

Fig. 17 Phase diagram $(z - z')$ for weak-strong simulation ($Q_x = 25.2$, $Q_z = 23.32$)

where $\underline{x}$ is the six-dimensional phase space vector of the coupled synchro-betatron motion. $\underline{A}$ and $\underline{\underline{B}}$ include the lattice nonlinearities, the beam-beam interaction and the average effect of the radiation. The term $\underline{\eta}$ is a stochastic vector process describing the stochastic emission of synchrotron radiation (quantum fluctuations). Depending on the stochastic process $\underline{\eta}$, $\underline{x}$ itself is a stochastic quantity specified by a distribution function $\varrho(\underline{x}, s)$ which is determined by the Fokker-Planck equation [38]:

$$\frac{\partial \varrho(\underline{x}, s)}{\partial s} = -\sum_i \frac{\partial}{\partial x_i}(A_i \varrho) + \frac{1}{2}\sum_{i,j,k} \frac{\partial}{\partial x_i}\left(B_{ik}\frac{\partial}{\partial x_j}(B_{jk}\varrho)\right). \tag{63}$$

The Fokker-Planck equation is a linear partial differential equation. A further discussion of this subject is beyond the scope of this lecture but can be found in Ref. [39].

In lepton colliders numerical simulations have been very helpful to get a better understanding of the beam-beam interaction, and in many cases a good agreement is found between numerical results and experiments. Electron-positron storage rings are strongly influenced by radiation effects. On the one side radiation causes damping of the particle oscillations while on the other – because of the stochastic emission of synchrotron light – these quantum fluctuations cause a stochastic excitation of the particle motion. After a few damping times the system has – hopefully – relaxed to its equilibrium. Tracking and numerical simulation of the particle motion can thus be limited to a few thousand revolutions corresponding to a few damping times.

The situation is quite different in present-day hadron colliders where radiation effects are almost negligible. Longtime predictions using numerical simulations are very subtle and CPU-time consuming. In this case, one is therefore strongly relying on analytical methods based on the theory of nonlinear (nonintegrable) Hamiltonian systems. We cannot cover this interesting field exhaustively, we can only illustrate some ideas and concepts. For further details the reader is referred to Refs. [7,40].

A model describing the weak-strong beam-beam interaction is given by the Hamiltonian

$$H = H_0 + H_1 \tag{64}$$

where

$$H_0 = \frac{p_x^2}{2} + k_x(s)\frac{x^2}{2} + \frac{p_z^2}{2} + k_z(s)\frac{z^2}{2} \tag{65}$$

describes the transverse linear betatron motion in an ideal uncoupled machine [28], and k_x, k_z are the horizontal and vertical focusing strength.

$$H_1 = U(x,z) \cdot \delta_p(s) \tag{66}$$

describes the nonlinear kick a test particle is experiencing when crossing the strong counter-rotating beam at the interaction point.

$$U(x,z) = \frac{N_b r_e}{\gamma} \int_0^\infty \frac{1 - \exp\left\{-\frac{x^2}{2\sigma_x^2+q} - \frac{z^2}{2\sigma_z^2+q}\right\}}{(2\sigma_z^2+q)^{1/2}(2\sigma_x^2+q)^{1/2}}\, dq \tag{14}$$

$\delta_p(s)$ is the periodic delta function

$$\delta_p(s) = \sum_n \delta(s - (s_{ip} + n \cdot C)) \tag{67}$$

(s_{ip} designates the interaction and C is the distance between adjacent interaction points).

The corresponding equations of motion read:

$$x' = \frac{\partial H}{\partial p_x} = p_x \tag{68a}$$

$$p_x' = -\frac{\partial H}{\partial x} = -k_x x - \frac{\partial U(x,z)}{\partial x} \cdot \delta_p(s) \tag{68b}$$

$$z' = \frac{\partial H}{\partial p_z} = p_z \tag{68c}$$

$$p_z' = -\frac{\partial H}{\partial z} = -k_z \cdot z - \frac{\partial U(x,z)}{\partial z} \cdot \delta_p(s). \tag{68d}$$

In order to find the solution to (68 a-d) from $s_{ip} - \varepsilon$ to $s_{ip} + C - \varepsilon$ (see Fig. 18) we proceed as follows:

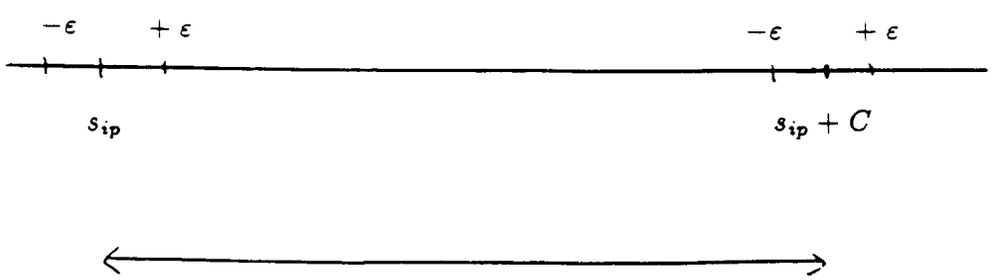

Fig. 18

The motion from $s_{ip} - \varepsilon$ to $s_{ip} + \varepsilon$ is just given by (kick):

$$\begin{pmatrix} x(s_{ip}+\varepsilon) \\ p_x(s_{ip}+\varepsilon) \\ z(s_{ip}+\varepsilon) \\ p_z(s_{ip}+\varepsilon) \end{pmatrix} = \begin{pmatrix} x(s_{ip}-\varepsilon) \\ p_x(s_{ip}-\varepsilon) - \frac{\partial U}{\partial x}(x(s_{ip}-\varepsilon), z(s_{ip}-\varepsilon)) \\ z(s_{ip}-\varepsilon) \\ p_z(s_{ip}-\varepsilon) - \frac{\partial U}{\partial z}(x(s_{ip}-\varepsilon), z(s_{ip}-\varepsilon)) \end{pmatrix} \tag{69}$$

or in shorthand notation

$$\underline{y}(s_{ip}+\varepsilon) = \underline{N}(\underline{y}(s_{ip}-\varepsilon)) \tag{70}$$

where $\underline{N}$ is a nonlinear four-dimensional map. From $s_{ip}+\varepsilon$ to $s_{ip}+C-\varepsilon$ the particle performs free (linear) betatron oscillations described by:

$$\begin{pmatrix} x(s_{ip}+C-\varepsilon) \\ p_x(s_{ip}+C-\varepsilon) \\ z(s_{ip}+C-\varepsilon) \\ p_z(s_{ip}+C-\varepsilon) \end{pmatrix} = \begin{pmatrix} \cos\mu_x & \beta^*_{0x}\sin\mu_x & 0 & 0 \\ -\frac{1}{\beta^*_{0x}}\sin\mu_x & \cos\mu_x & 0 & 0 \\ 0 & 0 & \cos\mu_z & \beta^*_{0z}\sin\mu_z \\ 0 & 0 & -\frac{1}{\beta^*_{0z}}\sin\mu_z & \cos\mu_z \end{pmatrix} \begin{pmatrix} x(s_{ip}+\varepsilon) \\ p_x(s_{ip}+\varepsilon) \\ z(s_{ip}+\varepsilon) \\ p_z(s_{ip}+\varepsilon) \end{pmatrix} \tag{71}$$

or

$$\underline{y}(s_{ip}+C-\varepsilon) = \underline{L}(\underline{y}(s_{ip}+\varepsilon)) \tag{72}$$

where $\underline{L}$ is a linear map (see Eq. (71)). The combined motion is given by inserting (69) into the right hand side of Eq. (71) or:

$$\underline{y}(s_{ip}+C-\varepsilon) = \underline{L}o\underline{N}(\underline{y}(s_{ip}-\varepsilon)). \tag{73}$$

Analysing the beam-beam interaction means investigating the nonlinear four-dimensional mapping (73) and its consequences for the particle motion. Numerical and perturbative methods have been developed to study these mappings, and it has turned out that these systems contain extremely complicated dynamics. In order to illustrate the problem and to demonstrate some of the unexpected features contained in

$$\underline{y}(n+1) = \underline{T}(\underline{y}(n)) \tag{74}$$

we make a further approximation. Since it is very difficult to visualize four-dimensional quantities we restrict ourselves to the two-dimensional case. This case describes, for example, the horizontal motion of a test particle which repeatedly crosses a round counter-rotating beam [41]:

$$x(n+1) = x(n)\cos\mu + \beta \cdot p(n) \cdot \sin\mu + \beta f(x(n)) \cdot \sin\mu \tag{75a}$$

$$p(n+1) = -\frac{1}{\beta}x(n)\sin\mu + p(n)\cos\mu + f(x(n))\cos\mu \tag{75b}$$

with

$$f(x) = -\frac{4\pi\xi}{\beta} x \, \frac{1 - \exp\,(-x^2/2\sigma^2)}{\frac{x^2}{2\sigma^2}} \tag{76}$$

(see Eq. (15)).

A numerical investigation of (75 a,b) is shown in Fig. 19 [9,41].

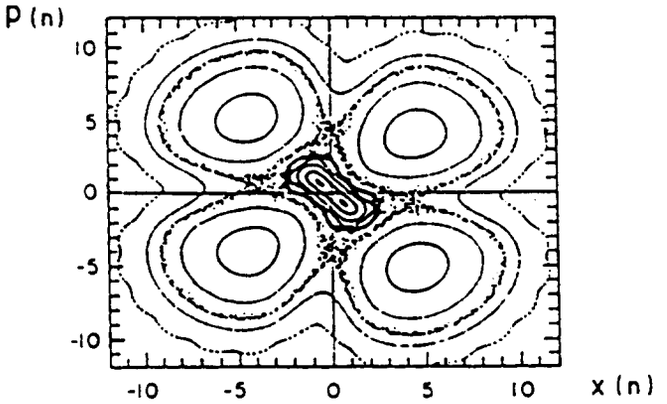

Fig. 19 Phase space plot of (75 a,b) for various initial conditions (x (o), p (o))

Depending on the initial conditions $(x(o), p(o))$ various orbits can be seen in this figure. There are closed regular trajectories, resonance islands corresponding to a rational tune $Q = r/s$ and chaotic trajectories. These chaotic orbits fill a certain area in phase space which increases with increasing nonlinearity. Extended chaotic regions appear if nonlinear resonances overlap. Two adjacent trajectories which start in this region will separate exponentially quickly in time. A detailed analysis of this kind of mapping [40]shows that regular and stochastic motion is mixed in an intricate manner in phase space. At this point a word of caution is in order. Two-dimensional maps are special in that the existence of closed regular trajectories (KAM orbits [40]) implies exact stability of motion. Since chaotic orbits cannot escape without intersecting these invariant curves, they are forever trapped inside. This is not true for higher-dimensional systems like our original mapping (73), where chaotic orbits can in principle always explore the whole four-dimensional phase space. Taking into account these results for nonlinear maps one hopes to be able to explain the beam-beam effects in hadron colliders. These effects are then related to the presence of extended chaotic regions in phase space or to diffusion effects induced by the beam-beam nonlinearities [7,41].

6. SUMMARY AND CONCLUSIONS

In this lecture we have tried to illustrate the problems related to the presence of two colliding beams in lepton and hadron storage rings. These beam-beam effects play an important role in all existing machines and a complete understanding is still missing.

All lepton colliders show a qualitatively similar behaviour concerning the current dependence of the luminosity and the beam-beam limit ξ. For all machines the upper limit of ξ is of the order of 0.07. In these colliders, numerical simulations taking into account the completely coupled synchro-betatron motion, radiation damping, quantum excitations and the nonlinear beam-beam interaction have led to a better understanding of the parameter dependence of

the system. In many cases, a good agreement is found between numerical calculations and experiments. Furthermore these simulations are the only method of treating the beam-beam interaction in a self-consistent manner so far, because the bunches will influence each other in a very complicated way. Analytical methods using concepts from the theory of stochastic differential equations are very difficult and are only at the beginning of their development.

In proton colliders nonlinear resonances play the dominant role in determining the luminosity. Even high-order nonlinear resonances must be avoided. Numerical simulations are very CPU-time consuming and subtle because of the lack of radiation damping. The longtime dynamics under the influence of the (nonlinear) beam-beam interaction can not be extrapolated easily from tracking the particles a few thousand revolutions. Therefore, in the hadron case one relies strongly on analytic (perturbative) methods of nonlinear (nonintegrable) Hamiltonian systems. The dynamics contained in these models shows a very rich and complicated structure: regular and chaotic regions are intricately mixed in phase space. In higher-dimensional systems (e.g. four-dimensional maps) various diffusion processes induced by the nonlinear character of the beam-beam interaction are possible. These include Arnold diffusion and various kinds of modulational diffusion [7,40]. The hope is that these concepts will explain the beam-beam effects in hadron colliders.

Until now, we have only considered colliders with head-on collisions. Machines with a crossing angle have to be treated with care. A detailed analysis of this case shows that the crossing angle induces a coupling between the synchrotron and betatron motion [21,42]. In this way, the number of nonlinear resonances is drastically increased

$$rQ_x + pQ_z + lQ_s = m. \tag{77}$$

This coupling is due to the fact that the kick a test particle experiences depends on its longitudinal position (see Fig. 20).

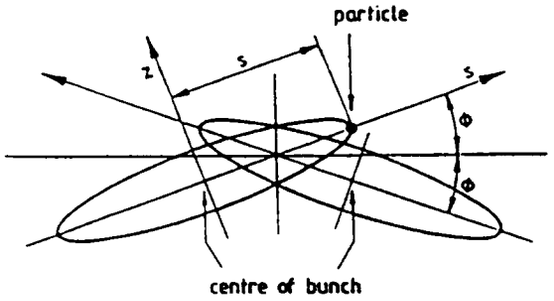

Fig. 20 Beam-beam interaction at a crossing angle

For further details and a comparison with experiments performed at DORIS I, the reader is referred to [18,42].

Another challenging problem not mentioned until now is the beam-beam interaction in linear colliders. Because of the extreme focusing of the beam to several square microns the deflecting fields for the particle will be very large, causing a variety of additional problems which we can only mention, such as beamstrahlung, pinch effect and other effects typical for plasmas. The reader can get an idea of the problem by looking at Fig. 21 which shows a numerical simulation of the pinch effect in linear colliders [43].

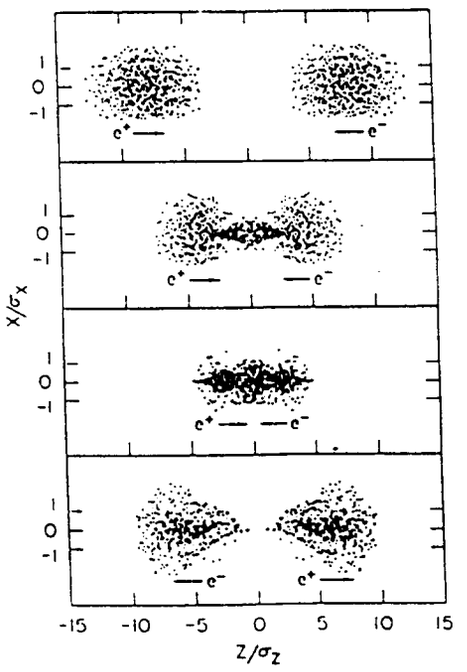

Fig. 21 Pinch effect in linear colliders

Summarizing, we can say that many experimental and theoretical facts are known. However, designing future colliders such as B-factories, which require an increase in luminosity by a factor 50 - 200 compared to the existing machines, or a linear collider is still very challenging. A good design has to rely on experimental observations, numerical simulations and, last but not least, on good theoretical models.

7. ACKNOWLEDGEMENT

We wish to thank S.G. Wipf for carefully reading the manuscript and A. Daum and M. Hoegemeier for their help with the references.

References

[1] M. Month, J.C. Herrera, eds., Nonlinear dynamics and the beam-beam interaction, Brookhaven National Laboratory (1979), AIP Conf. Proc. No. 57

[2] Proceedings of the beam-beam interaction seminar, SLAC-PUB-2624 (1980)

[3] I. Koop, G. Tumaikin, eds., Third advanced ICFA beam dynamics workshop on beam-beam effects in circular colliders, Novosibirsk (1989)

[4] L.R. Evans, J. Gareyte, Beam-beam effects, Proceedings CERN Accelerator School, Oxford 1985, CERN 87-03 (1987)

[5] P. Bambade, Effets faisceau-faisceau dans les annaux de stockage e^-/e^- à haute énergie: grossissement résonant des dimensions verticales dans le cas de faisceaux plats. LAL 84/21 (1984)

[6] J.F. Schonfeld, Beam-beam interaction, AIP Conf. Proc. No. 87

[7] J.L. Tennyson, The dynamics of the beam-beam interaction, AIP Conf. Proc. No. 87

[8] J.F. Schonfeld, The effects of beam-beam collisions on storage ring performance – a pedagogical review AIP Conf. Proc. No. 105

[9] A.W. Chao, Beam-beam instability, AIP Conf. Proc. No. 127

[10] E. Keil, Beam-beam interactions in p-p storage rings, CERN 77-13 (1977)

[11] G.H. Rees, Beam-beam interactions in e-p storage rings, ibid. [10]

[12] J. Le Duff, Beam-beam interactions in e^+e^- storage rings, ibid. [10]

[13] A.W. Chao, P. Bambade, W.T. Weng, Nonlinear beam-beam resonances, Lect. Notes in Physics Vol. 247, Springer (1986)

[14] J.T. Seeman, Observations of the beam-beam interaction, ibid. [13]

[15] S. Myers, Review of beam-beam simulations, ibid. [13]

[16] E. Keil, Beam-beam effects in electron and proton colliders, Part. Acc. 27, 165 (1990)

[17] J.R. Boyce, S. Heifets, G.A. Krafft, Simulations of high disruption colliding beams, CEBAF PR-90-013 (1990)

[18] A. Piwinski, Limitations of the luminosity by satellite resonances, DESY 77/18 (1977)

[19] A. Piwinski, Computer simulation of satellite resonances caused by the beam-beam interaction at a crossing angle in the SSC, SSC-57 (1986)

[20] A. Piwinski, Recent results from DORIS and PETRA in [1]

[21] A. Piwinski, Der Raumladungseffekt bei vertikalem oder horizontalem Kreuzungswinkel, DESY H1/1 (1969)

[22] J. Kewisch, Depolarisation der Elektronenspins in Speicherringen durch nichtlineare Spin-Bahn-Kopplung, DESY 85-109 (1985)

[23] P. Schmüser, Basic course on acclerator optics, Proceedings CERN Accelerator School, Aarhus, 1986, CERN 87-10 (1987)

[24] A. Piwinski, Coherent beam break-up due to space charge, Proc. 8th Intern. Conf. High Energy Accelerators, CERN (1971)

[25] A. Piwinski, Einstellung der Kreuzung der beiden Strahlen mit Hilfe des Raumladungseffekts, DESY H2-75/3 (1975)

[26] E. Courant, H. Snyder, Theory of the alternating gradient synchrotrons, Ann. Phys. 3, 1 (1958)

[27] G. Ripken, F. Willeke, On the impact of linear coupling on nonlinear dynamics, DESY 90-001 (1990)

[28] H. Mais, G. Ripken, Theory of coupled synchro-betatron oscillations (I), DESY M-82-05 (1982)

[29] H. Zyngier, Beam-beam effect – A review of the observations made at Orsay in [1]

[30] H. Wiedemann, Experiments on the beam-beam effect in e^+e^- storage rings in [1]

[31] D.A. Finley, Observations of beam-beam effects in proton-antiproton colliders in [3]

[32] A. Piwinski, Observation of beam-beam effects in PETRA, DESY M-79/11 (1979)

[33] A.W. Chao, R.D. Ruth, Coherent beam-beam instability in colliding-beam storage rings, Part. Accel. 16, 201 (1985)

[34] A. Piwinski, Computer simulation of beam-beam interaction for various betatron frequencies, DESY M-81/31 (1981)

[35] S. Peggs, R. Talman, Beam-beam luminosity limitation in electron-positron colliding rings, Phys. Rev. D24, 2379 (1981)

[36] S. Myers, Simulation of the beam-beam effect for e^+e^- storage rings, Nucl. Instr. Meth. 211, 263 (1983)

[37] A. Piwinski, Dependence of the luminosity on various machine parameters and their optimization at PETRA, DESY 83-028 (1983)

[38] C.W. Gardiner, Handbook of stochastic methods, Springer (1985)

[39] A.L. Gerasimov, Phase convection and distribution "tails" in periodically driven Brownian motion, Physica D41, 89 (1990)

[40] A.J. Lichtenberg, M.A. Lieberman, Regular and stochastic motion, Springer (1983)

[41] F.M. Izraelev, Nearly linear mappings and their applications, Physica D1, 243 (1980)

[42] A. Piwinski, Synchro-betatron resonances in [4]

[43] R. Hollebeek, Disruption limits for linear colliders, in [2]